

All-Optical GeV Electron Bunch Generation in a Laser-Plasma Accelerator via Truncated-Channel Injection


A. Picksley^{1,*}, J. Chappell¹, E. Archer¹, N. Bourgeois², J. Cowley¹, D. R. Emerson³, L. Feder¹, X. J. Gu³,
O. Jakobsson^{1,†}, A. J. Ross¹, W. Wang¹, R. Walczak^{1,4} and S. M. Hooker^{1,‡}

¹*John Adams Institute for Accelerator Science and Department of Physics, University of Oxford,
Denys Wilkinson Building, Keble Road, Oxford OX1 3RH, United Kingdom*

²*Central Laser Facility, STFC Rutherford Appleton Laboratory, Didcot OX11 0QX, United Kingdom*

³*Scientific Computing Department, STFC Daresbury Laboratory, Warrington WA4 4AD, United Kingdom*

⁴*Somerville College, Woodstock Road, Oxford OX2 6HD, United Kingdom*

 (Received 24 July 2023; revised 11 October 2023; accepted 7 November 2023; published 12 December 2023)

We describe a simple scheme, truncated-channel injection, to inject electrons directly into the wakefield driven by a high-intensity laser pulse guided in an all-optical plasma channel. We use this approach to generate dark-current-free 1.2 GeV, 4.5% relative energy spread electron bunches with 120 TW laser pulses guided in a 110 mm-long hydrodynamic optical-field-ionized plasma channel. Our experiments and particle-in-cell simulations show that high-quality electron bunches were only obtained when the drive pulse was closely aligned with the channel axis, and was focused close to the density down ramp formed at the channel entrance. Start-to-end simulations of the channel formation, and electron injection and acceleration show that increasing the channel length to 410 mm would yield 3.65 GeV bunches, with a slice energy spread $\sim 5 \times 10^{-4}$.

DOI: 10.1103/PhysRevLett.131.245001

It has become well established that laser-plasma accelerators (LPAs) [1] can accelerate few femtosecond [2–6] electron bunches to GeV-scale energies in accelerator stages only a few centimetres long [7–13]. These highly desirable features make LPAs attractive for driving compact, femtosecond-duration light sources [14,15], including free-electron lasers (FELs). FEL gain has recently been reported in experiments utilizing laser- [16,17] and beam-driven [18,19] plasma accelerators. Other work has demonstrated generation of incoherent soft x radiation in an undulator [20], and at photon energies in the keV range from betatron oscillations [21], and at MeV energies from Thomson scattering [22–24].

These demanding applications require generation of multi-GeV electron bunches with high peak current, low transverse emittance, and small shot-to-shot jitter of the bunch properties. Therefore, it is preferable to operate in the linear, or quasilinear, regime [25] in order to prevent uncontrolled self-injection at one or more points along the length of the accelerator. However, this regime brings two significant challenges. First, relativistic self-focusing does not occur and hence the drive laser pulse must be guided over several Rayleigh lengths to reach multi-GeV energies. Second, trapping of electrons is more difficult since the electric fields of the plasma wave are lower than in the highly nonlinear regime [25].

In order to meet the first of these challenges, we have developed low-density hydrodynamic optical-field-ionized (HOFI) plasma channels [26–29], building on pioneering work by Milchberg *et al.* [30–33]. These channels have low

losses, and could in principle be several meters long [34]. Experiments have demonstrated guiding of relativistically intense laser pulses through 200 mm-long channels with axial densities as low as $1 \times 10^{17} \text{ cm}^{-3}$ [34–37], and operation at kHz pulse repetition rates [38].

In this Letter we demonstrate a new approach that addresses both challenges in a single stage. We show that the density down ramp formed at the start of a HOFI channel promotes electron injection directly into the quasilinear wakefield driven by a channel-guided drive pulse. We demonstrate experimentally that this truncated-channel injection (TCI) scheme produces electron bunches with an energy up to 1.2 GeV, and a root-mean-square (rms) energy spread of $\sigma_E/\mu_E = 4.5\%$ with 120 TW laser pulses. We show that high-quality TCI bunches are only generated when the drive laser is (i) focused close to the down ramp at the channel entrance, and (ii) well aligned with, and hence guided by, the HOFI channel. In contrast, we find that bunches produced by ionization injection have much larger energy spread and are preferentially generated when the drive pulse is misaligned with the channel. The experimental results are found to be in excellent agreement with start-to-end simulations of the complete TCI scheme, which includes hydrodynamic simulations of the formation of the HOFI channel and high-resolution particle-in-cell (PIC) simulations of electron injection and acceleration. These simulations show that dephasing was not reached in our experiments, and that extending the channel length to the dephasing length $L_d \approx 410 \text{ mm}$ would yield bunches of energy 3.65 GeV, a slice energy spread below the per-mille

level, a peak current of 0.8 kA, and a normalized transverse emittance of $\epsilon_{n,\perp} < 5$ mm mrad. These properties appear well matched to the requirements of soft x-ray FELs driven by 100 TW class lasers.

Before describing this Letter in detail we note that Scott *et al.* [39] investigated electron injection in a prepulse generated plasma structure similar to that investigated here, but not coupled into a waveguide. Oubrerie *et al.* generated 1.1 GeV bunches with relative energy spread 4%, following blade-induced shock injection in a higher-density, 15-mm-long, all-optical channel [40]. Miao *et al.* used 300 TW laser pulses to generate 5 GeV bunches with large energy spreads following ionization injection in nitrogen-doped, 20-cm-long HOFI channels [41]. Recent work investigating density transitions generated by hydrodynamically expanding shocks has demonstrated their feasibility for beam-driven [42] and laser-driven [43] acceleration.

Figure 1 outlines the TCI scheme, and the experimental arrangement employed using the Astra-Gemini TA3 Ti: sapphire laser at the Rutherford Appleton Laboratory which delivers (47 ± 3) fs pulses with $\lambda_0 = 800$ nm. The channel-forming beam, of pulse energy (86 ± 17) mJ, was focused by an axicon lens to form a plasma column within the 110-mm-long gas target. The drive beam, containing (5.8 ± 0.2) J, was focused into the gas target to a spot-size $w_0 \approx 40$ μm , with peak intensity $I_{\text{pk}} \approx 2.4 \times 10^{18}$ W cm^{-2} ($a_0 \approx 1.0$). The delay between the arrival of the two pulses was set to $\Delta\tau = 3.5$ ns. The target comprised a 110 mm long hybrid gas jet cell [44] filled with a 2% mix of nitrogen in hydrogen.

A small fraction ($< 1\%$) of the drive laser was transmitted through the final turning mirror and focused in order to measure on each shot the input transverse offset, δr , of the drive pulse focus relative to the channel. After leaving the cell, the drive pulse was directed to a far-field camera, and two fiber-based optical spectrometers. Electron beam characteristics were measured by an electron spectrometer.

Truncating the plasma channel to trigger injection was achieved by delaying the longitudinal position of the start of the HOFI plasma channel z_{ch} as follows. In principle z_{ch} is calculated from the diameter (26 mm) of the central hole in the axicon and the approach angle of the axicon (1.6°). In practice, however, wavefront nonuniformities and diffraction determine the distance over which the intensity of the line focus increases from zero to the threshold intensity for ionization. Figure 1(b) shows the measured intensity distribution, $I_{\text{ax}}(r, z)$, near the start of the axicon line focus, and Fig. 1(c) shows the calculated electron temperature profile $T_e(r, z)$ of the resulting initial plasma column [45]. The strong intensity dependence of optical field ionization causes the onset of the plasma column to be significantly sharper than that of $I_{\text{ax}}(r, z)$. Hydrodynamic simulations [see Fig. 1(d)] show that the front edge of the plasma column expands longitudinally to form a hemispherical acoustic shock wave, resembling a Sedov-Taylor *spherical* expansion

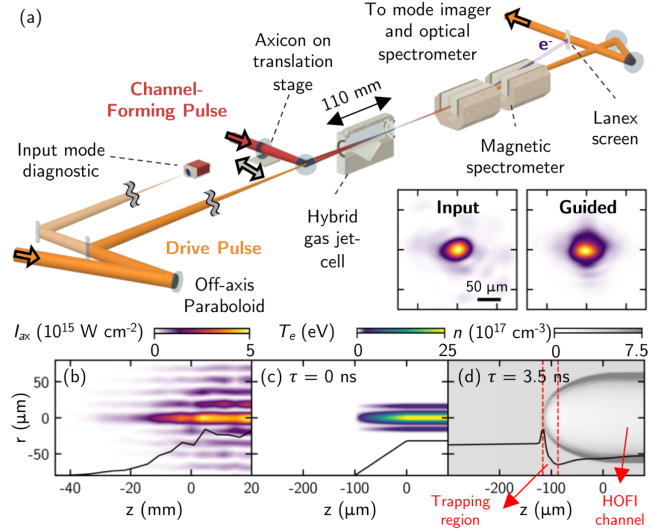


FIG. 1. Schematic of truncated-channel injection scheme. (a) Setup: channel-forming (red) and drive (orange) beams were coupled into the gas target. The input mode, output mode, optical, and electron spectra were measured on every shot. Inset: measured transverse fluence profiles of the drive laser at focus and at the exit of the HOFI channel. (b) Measured axicon longitudinal intensity profile, (c) calculated initial electron temperature profile, and (d) calculated density profile of the truncated HOFI plasma channel 3.5 ns after arrival of the channel-forming pulse. In each panel, the black curve shows the relative magnitude of each variable along the optical axis.

of electron and neutral density ($n = n_e + n_{\text{H}}$) [45,56]. The body of the plasma column expands radially, driving a *cylindrical* shock into the surrounding gas [28,34]. The leading edge of the drive laser will ionize any neutral atoms to give a new electron density equal to n [34,37]. The scale length of the transition, $\hat{L}_{\text{tr}} = n_{e0}/(dn_e/dz)$, where n_{e0} is the axial density in the HOFI channel, is varied by adjusting the position of z_{ch} within the plume of gas exiting the cell entrance. Since the expansion rates of the hemispherical and cylindrical blast waves are different, independent control over the parameters of the injection and acceleration section can be achieved (see the Appendix). The calculated $\hat{L}_{\text{tr}} \approx 15$ μm is short compared to the plasma wavelength $\lambda_p = 2\pi c(n_{e0}e^2/m_e\epsilon_0)^{-1/2} \approx 100$ μm , hence localized injection is triggered by an abrupt change in wakefield phase as the plasma electrons cross the density transition [57–59].

We examined the TCI scheme by setting the longitudinal position of the drive pulse focus, z_f , to coincide with the position of the front pinhole, and varying z_{ch} so as to adjust their separation, $\Delta z = z_{\text{ch}} - z_f$, between -11.2 mm and 0.8 mm. We note that in a standard guiding experiment $\Delta z \ll 0$ mm, so that the entrance to the channel is far upstream of the drive pulse focus. The axial plasma density was set to $\sim (1.3 \pm 0.1) \times 10^{17}$ cm^{-3} , suppressing ionization injection for guided pulses [45] when $\Delta z = -11.2$ mm.

Figure 2(a) shows the recorded injection probability, p_{inj} , as a function of Δz , where injection is considered to have

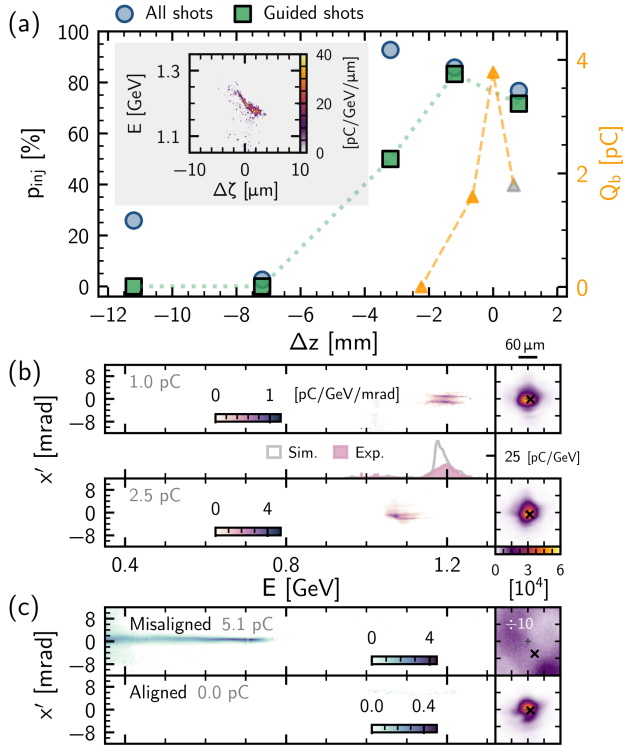


FIG. 2. (a) Left axis: injection probability, p_{inj} , as a function of $\Delta z = z_{\text{ch}} - z_f$ for all (blue circles) and guided (green squares) shots. Right axis: variation of calculated electron bunch charge Q_b with Δz , from PIC simulations. Inset (gray): simulated longitudinal phase-space distribution of the electron bunch at the channel exit for $\Delta z = 0.8$ mm. (b) Examples of the measured, angularly resolved, electron spectra (left) and guided drive beam profile (right) for $\Delta z = 0.8$ mm; black crosses show the drive input position. Also shown is a comparison between the measured and simulated spectral density. (c) Plots as in (b) for $\Delta z = -11.2$ mm, for cases where the drive pulse was misaligned (upper) or aligned (lower) to the channel.

occurred if the total charge recorded by the electron spectrometer exceeded 0.05 pC. For guided shots, electron bunches were observed for $-3.2 \text{ mm} \leq \Delta z \leq 0.8 \text{ mm}$, i.e. when the drive focus was well within one Rayleigh length of the leading edge of the plasma channel. For 124 guided shots with $\Delta z \geq -3.2 \text{ mm}$, $p_{\text{inj}} = 74\%$, whereas no electron injection was observed in 73 guided shots when $\Delta z \leq -7.2 \text{ mm}$. With the channel entrance at its most downstream position, $\Delta z = 0.8 \text{ mm}$, high-quality guiding and electron acceleration were observed simultaneously when the input beam was well aligned with the HOPI channel, as shown in Fig. 2(b). Electron bunches of pC-scale charge with mean energies in excess of 1 GeV and few-percent energy spreads were consistently observed for input offsets $\delta r \lesssim 10 \mu\text{m}$. These shots exhibited an angular splitting of the bunch; PIC simulations indicated that this arose from transverse oscillations of the bunch that are seeded by laser mode beating [45]. When the channel entrance was upstream of the drive focus ($\Delta z \leq -7.2 \text{ mm}$),

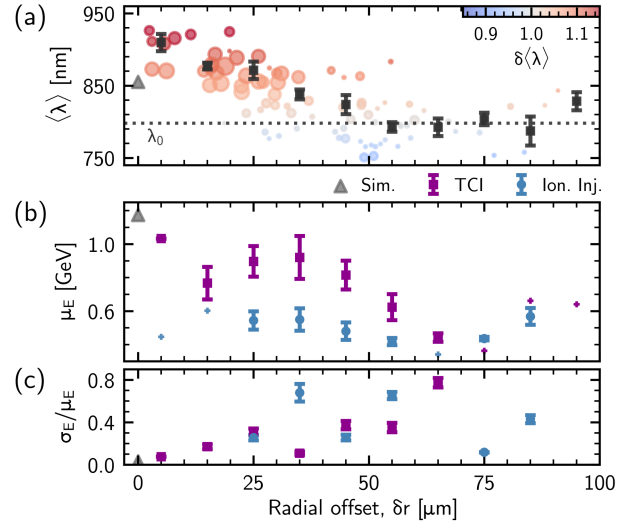


FIG. 3. Variation with δr of the spectra of the output drive and electron beams. (a) $\langle \lambda \rangle$ for $\Delta z = 0.8 \text{ mm}$. The size of data points corresponds to the relative fluence of the measured guided mode. The result from start-to-end simulations is shown in gray. (b) Mean electron energy, μ_E , for guided shots for TCI (purple squares) and ionization injection (blue circles); bins containing only a single event use “+” markers. For the ionization injection dataset, $\Delta z = -11.2 \text{ mm}$ and $n_{e0} = (2.2 \pm 0.1) \times 10^{17} \text{ cm}^{-3}$. (c) Average ratio σ_E/μ_E of accelerated electron bunches. For all plots the data points with error bars are averages over 10 μm -wide bins [45], with the error bars showing one standard error.

electron injection was not observed for guided shots, and instead injection was only observed when the drive pulse was offset transversely from the channel axis [see Fig. 2(c)].

The spectral shift of the drive pulses provides insight into wakefield excitation along the plasma channel. Figure 3(a) shows, as a function of δr , the intensity-weighted average wavelength, $\langle \lambda \rangle$, of the transmitted drive pulse, together with a measure of the wavelength shift, $\delta \langle \lambda \rangle = \langle \lambda \rangle / \lambda_0$. Well-aligned shots ($\delta r \lesssim 30 \mu\text{m}$) are strongly correlated with high transmission and significant red-shifting, corresponding to good guiding and strong wakefield excitation. In contrast, shots with large δr are strongly associated with low transmission and significant blue-shifting, consistent with significant ionization by the drive pulse.

Figures 3(b) and 3(c) show corresponding effects in the measured electron energies, with larger mean energies μ_E measured for smaller δr . As shown in Fig. 3(c), well-aligned shots ($\delta r \leq 10 \mu\text{m}$) have dramatically lower relative rms energy spread— $\sigma_E/\mu_E \approx 7\%$ on average, with a best of 4.5%—than less well-aligned shots. Furthermore, well-aligned shots exhibited percent-level shot-to-shot energy stability, with a mean energy of $\mu_E = (1.033 \pm 0.010) \text{ GeV}$. For larger input offsets ($10 < \delta r \leq 50 \mu\text{m}$), electron bunches of higher charge ($\sim 10 \text{ pC}$) were obtained with spectra typically comprising multiple peaks superposed on a continuous spectrum

extending to $\lesssim 1.0$ GeV, with a mean energy $\mu_E \sim 0.8$ GeV. For $\delta r > 50$ μm , electron spectra were effectively continuous, with $\mu_E \sim 0.5$ GeV.

Figures 3(b) and 3(c) also show results for the case of ionization injection from the nitrogen dopant, which was studied by setting $n_{e0} = (2.2 \pm 0.1) \times 10^{17}$ cm^{-3} and translating the axicon to $\Delta z = -11.2$ mm. It is noticeable that for ionization injection μ_E is lower and much less sensitive to δr . Electrons were preferentially injected when the drive pulse was slightly misaligned with respect to the axis of the channel. Injection occurred only twice in 26 shots with $\delta r \leq 20$ μm ($\sim 7\%$) but occurred in $\sim 30\%$ of guided events for $20 < \delta r \leq 50$ μm .

The data presented in Figs. 2 and 3 may be interpreted as follows. At the lower density investigated in this Letter, high quality electron injection only occurred when the drive pulses were (i) well aligned with the channel ($\delta r < 10$ μm), and (ii) focused close to the channel entrance ($\Delta z = 0.8$ mm). For these conditions, strong wakefield excitation occurred, and ~ 1 GeV electron bunches with few-percent energy spread were generated with an injection probability of $\sim 80\%$. When the channel entrance was located far upstream of the drive focus, electron bunches were only generated if the drive pulse was misaligned; in this case, the electron spectra were broadband, and the transmitted drive pulses had low energy transmission with much reduced red-shifting. These observations are consistent with poorly-aligned drive pulses interacting with the higher-density channel walls and surrounding neutral gas, triggering uncontrolled electron injection, potentially at several points along the channel. For the case of ionization injection, broadband electron bunches were generated for a wide range of δr , suggesting that high-quality guiding was not necessary, and that injection occurred at several points along the plasma channel.

To gain further insight we performed start-to-end modelling of the channel formation and electron acceleration process [45]. An Airy drive laser focus with $\delta r = 0$ and other parameters similar to the experiment was assumed. The right-hand axis of Fig. 2(a) shows the calculated electron bunch charge Q_b at the channel exit for several values of Δz . The variation of Q_b with Δz is qualitatively similar to p_{inj} , although the range of Δz over which injection is observed in simulation is smaller. The inset to this figure shows the calculated longitudinal phase space of the bunch at the exit of the channel for $\Delta z = 0.8$ mm. The properties of this bunch are $\mu_E = 1.175$ GeV, $\sigma_E = 38$ MeV (3.2%), and $Q_b = 1.8$ pC. The calculated FWHM bunch duration was 9.4 fs, and the mean slice energy spread was $(1.0 \pm 0.4)\%$. The spectra of the electron bunch and the transmitted drive pulse are found to be in good agreement with the measurements [see Figs. 2(b) and 3(a)].

Efficient coupling of the drive pulse and electron bunch into the HOFI channel depended on w_0 and z_f . For the conditions of Fig. 2, approximately 20% of the trapped

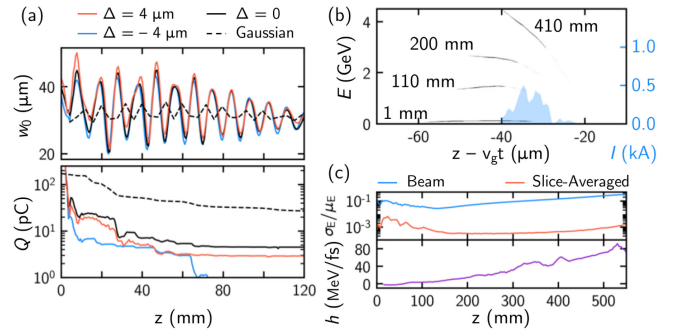


FIG. 4. (a) Laser spot size (top) and TCI bunch charge (bottom) during propagation for input modes of different sizes. (b) Electron bunch longitudinal phase space at four different propagation distances. The longitudinal current profile at $z = 410$ mm is shown in blue. (c) Relative energy spread of the TCI bunch (σ_E/μ_E , blue), the mean relative slice energy spread (red), and bunch chirp (h , purple).

charge was coupled into the channel, the rest being immediately dephased. Rapid spot-size oscillations, caused by improper matching of the drive pulse into the HOFI channel, led to transverse ejection of particles from the wakefield. Figure 4(a) shows the evolution with z of the mode size $w(z)$ and Q_b for the same channel parameters as Fig. 2 and several Airy input modes mismatched to the channel by $\Delta = w_m - w_0$. For a Gaussian mode with $w_0 \approx w_m$, $> 40\%$ of injected bunch charge is transported into the channel, increasing the peak current by an order of magnitude compared to the Airy mode.

Figure 4 also shows the evolution of the bunch characteristics for channels with a length up to the dephasing length $L_d \approx 410$ mm, i.e. longer than investigated here, but experimentally feasible [34,37]. At $z = L_d$, the properties of the bunch are found to be $\mu_E = 3.65$ GeV; $\sigma_E = 487$ MeV ($\sigma_E/\mu_E = 13.3\%$); an rms duration of ~ 26 fs, corresponding to a peak current $I_{\text{peak}} \approx 0.7$ kA; and a normalized projected transverse emittance of $\epsilon_{n,\perp} \approx 5.8$ mm mrad (with a slice average of $\epsilon_{n,\perp}^{\text{slice}} \approx 3.6$ mm mrad).

Evolution of the bunch chirp, $h(z)$, is shown in Fig. 4(c). Upon injection, TCI bunches exhibit negative chirp ($h \approx -1.2$ MeV fs^{-1}); during propagation the accelerating field causes h to increase to ≈ 49 MeV fs^{-1} . Thanks to the linear longitudinal phase-space distribution, a plasma-based dechirper [60] could reduce σ_E to the level of the slice-averaged energy spread, $\sigma_E^{\text{slice}}/\mu_E \sim 5.0 \times 10^{-4}$, potentially producing an FEL-quality bunch. In the 1D limit, three bunch conditions must be satisfied [61], of which we find the most stringent is $\epsilon_{\perp} = \epsilon_{n,\perp}^{\text{slice}}/\gamma < \lambda_R/4\pi$, where γ is the Lorentz factor and λ_R is the FEL wavelength. This results in $\lambda_R \gtrsim 4\pi\epsilon_{\perp} \approx 6$ nm, making the TCI scheme appealing to such applications. Alternatively, bunch compression could result in sub-fs, $\gtrsim 10$ kA peak current bunches; similar schemes have been proposed for generating high peak power, attosecond-duration soft x rays from plasma-based accelerators [62].

In summary, we have demonstrated a simple scheme to inject electrons directly into the wakefield driven by a pulse guided by an all-optical plasma channel. Dark-current-free, 1.2 GeV bunches with 4.5% relative energy spread were generated with 120 TW laser pulses guided in a 110 mm-long HOFI plasma channel. Our measurements, supported by simulations, showed that high-quality electron bunches were only obtained when the drive pulse was well aligned with the channel axis and focused close to the density down ramp formed at the channel entrance, and that increasing the channel length to $L_d \approx 410$ mm would yield 3.65 GeV bunches, with relative slice energy spread below the permille level. In contrast, bunches injected via ionization were broadband and preferentially occurred when the drive was misaligned with the channel. This experiment is the first to exploit sculpting of the longitudinal and transverse density profile of all-optical plasma channels to control electron injection into a plasma channel accelerator stage. Further tailoring of the plasma channel could be achieved by manipulating the channel-forming pulse itself, or employing additional laser pulses. All techniques employed here are well suited to \gtrsim kHz repetition rates, making this scheme promising for high-repetition-rate, compact radiation sources, including FELs.

The authors would like to acknowledge useful discussions with Rémi Lehe. This work was supported by the UK Science and Technology Facilities Council (STFC UK), Grants No. ST/R505006/1, No. ST/S505833/1 and No. ST/V001655/1; the Engineering and Physical Sciences Research Council, Grants No. EP/R513295/1 and No. EP/V006797/1; and the Central Laser Facility of the United Kingdom. This material is based upon work supported by the Air Force Office of Scientific Research under Award No. FA9550-18-1-7005. Computing resources provided by STFC Scientific Computing Department's SCARF cluster. The CFD work used in this study was supported by funding from the CLF/EPAC (Extreme Photonics Applications Centre). The software used in this work was developed in part by the DOE NNSA and DOE Office of Science-supported Flash Center for Computational Science at the University of Chicago and the University of Rochester. This research was funded in whole, or in part, by EPSRC and STFC, which are Plan S funders.

Appendix: Control over the density transition and channel characteristics.—It is important to be able to control the scale length of the longitudinal density transition, $\hat{L}_{tr} = n_{e0}/(dn_e/dz)$, since this determines properties of the injected electron bunch. Furthermore, having independent control over the injector and accelerator section is vital for producing high quality electron bunches. Even though TCI uses a single laser pulse to both create the down ramp and the plasma channel, it offers additional control and benefits over

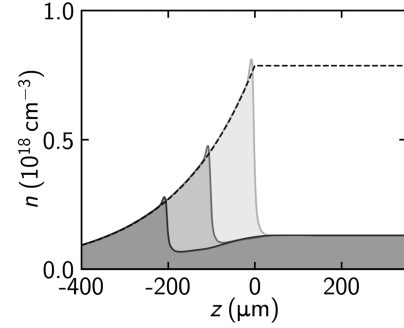


FIG. 5. Results of fluid simulations of the longitudinal variation of the total density $n = n_e + n_H$ for three simulations with $T_e(r, z - \delta z)$ with $\delta z = 0, -100, -200 \mu\text{m}$. The initial gas density profile, n_{gas} , assumed in these simulations is represented by the black dashed line.

schemes where shocks are generated by interrupting the flow of gas [63–65].

With the TCI scheme, \hat{L}_{tr} is achieved by fixing the position of the gas cell entrance ($z = 0$) and varying the position of the start of the axicon focus z_{ch} within the gas plume. Figure 5 illustrates this tunability, showing the longitudinal density profile $n(z) = (n_e + n_H)$ calculated via magnetohydrodynamic simulations [45] for a fixed initial gas density distribution and $T_e(r, z - \delta z)$, with $\delta z = 0, -100, -200 \mu\text{m}$ where $T_e(r, z)$ is shown in Fig. 1(c). The black dashed line indicates n_{gas} at $\tau = 0$. It can be seen

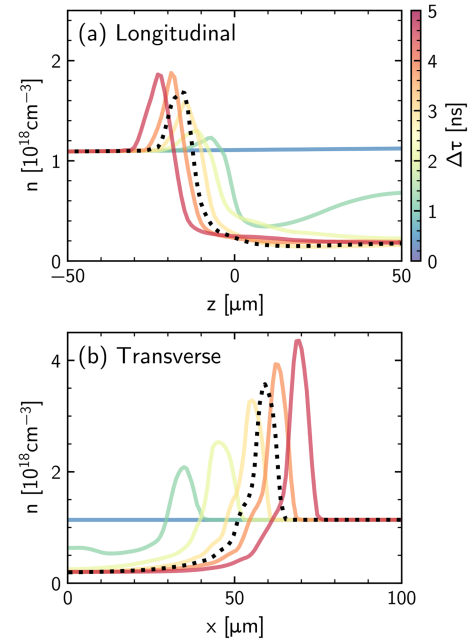


FIG. 6. Results of fluid simulations showing the temporal evolution of the total density $n = n_e + n_H$ for (a) the longitudinal expansion at the start of the channel and (b) the transverse expansion of the bulk that forms the guiding structure. The delays plotted vary between 0 and 5 ns in steps of 1 ns. The delay used in the experiment, $\Delta\tau = 3.5$ ns, is represented by the black dotted line.

that the down-ramp length is $\approx 70 \mu\text{m}$ and the ratio of the peak shock density to the on-axis density in the main part of the channel, n_{shock}/n_{e0} can be varied from approximately 2 to 6, corresponding to a variation of $\hat{L}_{\text{tr}} = 70\text{--}15 \mu\text{m}$, and thus allowing sufficient control over the injected electron bunch properties.

Additionally, while the time delay $\Delta\tau$ between the two pulses determines the channel size and matching condition for the propagation section, it does not affect the properties of \hat{L}_{tr} for $\Delta\tau$ where guiding profiles exist. Figure 6 shows the evolution of both the longitudinal expansion of the leading edge of the channel and the transverse expansion of the bulk. The hemispherical expansion responsible for the injection section carries less energy-per-unit length compared to the cylindrical expansion of the channel body. After 3 ns the shape of this transition is essentially unchanged, except for a small longitudinal shift. Over the same time period, the transverse expansion of the bulk continues, modifying the shape of the guiding channel and hence its matched spot size. This difference in expansion rate allows independent tuning of the injection region and guiding properties of the channel, without the need to modify the gas target.

*apicksley@lbl.gov

Present address: Lawrence Berkeley National Laboratory, Berkeley, California 94720, USA.

†Deceased.

‡simon.hooker@physics.ox.ac.uk

- [1] T. Tajima and J. M. Dawson, Laser electron accelerator, *Phys. Rev. Lett.* **43**, 267 (1979).
- [2] J. Van Tilborg, C. Schroeder, C. Filip, C. Tóth, C. Geddes, G. Fubiani, R. Huber, R. Kaindl, E. Esarey, and W. Leemans, Temporal characterization of femtosecond laser-plasma-accelerated electron bunches using terahertz radiation, *Phys. Rev. Lett.* **96**, 014801 (2006).
- [3] T. Ohkubo, A. Maekawa, R. Tsujii, T. Hosokai, K. Kinoshita, K. Kobayashi, M. Uesaka, A. Zhidkov, K. Nemoto, Y. Kondo, and Y. Shibata, Temporal characteristics of monoenergetic electron beams generated by the laser wakefield acceleration, *Phys. Rev. ST Accel. Beams* **10**, 031301 (2007).
- [4] A. D. Debus *et al.*, Electron bunch length measurements from laser-accelerated electrons using single-shot THz time-domain interferometry, *Phys. Rev. Lett.* **104**, 084802 (2010).
- [5] O. Lundh, J. Lim, C. Rechatin, L. Ammoura, A. Ben-Ismaïl, X. Davoine, G. Gallot, J. P. Goddet, E. Lefebvre, V. Malka, and J. Faure, Few femtosecond, few kiloampere electron bunch produced by a laser-plasma accelerator, *Nat. Phys.* **7**, 219 (2011).
- [6] M. Heigoldt, A. Popp, K. Khrennikov, J. Wenz, S.-W. Chou, S. Karsch, S. I. Bajlekov, S. M. Hooker, and B. Schmidt, Temporal evolution of longitudinal bunch profile in a laser wakefield accelerator, *Phys. Rev. ST Accel. Beams* **18**, 121302 (2015).
- [7] W. P. Leemans, B. Nagler, A. J. Gonsalves, C. Tóth, K. Nakamura, C. G. R. Geddes, E. Esarey, C. B. Schroeder, and S. M. Hooker, GeV electron beams from a centimetre-scale accelerator, *Nat. Phys.* **2**, 696 (2006).
- [8] S. Karsch, J. Osterhoff, A. Popp, T. P. Rowlands-Rees, Z. Major, M. Fuchs, B. Marx, R. Hörlein, K. Schmid, L. Veisz, S. Becker, U. Schramm, B. Hidding, G. Pretzler, D. Habs, F. Grüner, F. Krausz, and S. M. Hooker, GeV-scale electron acceleration in a gas-filled capillary discharge waveguide, *New J. Phys.* **9**, 415 (2007).
- [9] X. Wang, R. Zgadzaj, N. Fazel, Z. Li, S. A. Yi, X. Zhang, W. Henderson, Y. Y. Chang, R. Korzekwa, H. E. Tsai, C. H. Pai, H. Quevedo, G. Dyer, E. Gaul, M. Martinez, A. C. Bernstein, T. Borger, M. Spinks, M. Donovan, V. Khudik, G. Shvets, T. Ditmire, and M. C. Downer, Quasi-monoenergetic laser-plasma acceleration of electrons to 2 GeV, *Nat. Commun.* **4**, 1988 (2013).
- [10] W. P. Leemans, A. J. Gonsalves, H. S. Mao, K. Nakamura, C. Benedetti, C. B. Schroeder, C. Toth, J. Daniels, D. E. Mittelberger, S. S. Bulanov, J. L. Vay, C. G. R. Geddes, and E. Esarey, Multi-GeV electron beams from capillary-discharge-guided subpetawatt laser pulses in the self-trapping regime, *Phys. Rev. Lett.* **113**, 245002 (2014).
- [11] J. Shin, H. T. Kim, V. B. Pathak, C. Hojibota, S. K. Lee, J. H. Sung, H. W. Lee, J. W. Yoon, C. Jeon, K. Nakajima, F. Sylla, A. Lifschitz, E. Guillaume, C. Thauray, V. Malka, and C. H. Nam, Quasi-monoenergetic multi-GeV electron acceleration by optimizing the spatial and spectral phases of PW laser pulses, *Plasma Phys. Controlled Fusion* **60**, 064007 (2018).
- [12] A. J. Gonsalves *et al.*, Petawatt laser guiding and electron beam acceleration to 8 GeV in a laser-heated capillary discharge waveguide, *Phys. Rev. Lett.* **122**, 084801 (2019).
- [13] L. Ke, K. Feng, W. Wang, Z. Qin, C. Yu, Y. Wu, Y. Chen, R. Qi, Z. Zhang, Y. Xu *et al.*, Near-gev electron beams at a few per-mille level from a laser wakefield accelerator via density-tailored plasma, *Phys. Rev. Lett.* **126**, 214801 (2021).
- [14] S. Corde, C. Thauray, A. Lifschitz, G. Lambert, K. Ta Phuoc, X. Davoine, R. Lehe, D. Douillet, A. Rousse, and V. Malka, Observation of longitudinal and transverse self-injections in laser-plasma accelerators, *Nat. Commun.* **4**, 1501 (2013).
- [15] F. Albert and A. G. Thomas, Applications of laser wakefield accelerator-based light sources, *Plasma Phys. Controlled Fusion* **58**, 103001 (2016).
- [16] W. Wang, K. Feng, L. Ke, C. Yu, Y. Xu, R. Qi, Y. Chen, Z. Qin, Z. Zhang, M. Fang, J. Liu, K. Jiang, H. Wang, C. Wang, X. Yang, F. Wu, Y. Leng, J. Liu, R. Li, and Z. Xu, Free-electron lasing at 27 nanometres based on a laser wakefield accelerator, *Nature (London)* **595**, 516 (2021).
- [17] M. Labat *et al.*, Seeded free-electron laser driven by a compact laser plasma accelerator, *Nat. Photonics* **17**, 150 (2022).
- [18] R. Pompili *et al.*, Free-electron lasing with compact beam-driven plasma wakefield accelerator, *Nature (London)* **605**, 659 (2022).
- [19] M. Galletti *et al.*, Stable operation of a free-electron laser driven by a plasma accelerator, *Phys. Rev. Lett.* **129**, 234801 (2022).
- [20] M. Fuchs, R. Weingartner, A. Popp, Z. Major, S. Becker, J. Osterhoff, I. Cortie, B. Zeitler, R. Hörlein, G. D. Tsakiris,

- U. Schramm, T. P. Rowlands-Rees, S. M. Hooker, D. Habs, F. Krausz, S. Karsch, and F. Grüner, Laser-driven soft-x-ray undulator source, *Nat. Phys.* **5**, 826 (2009).
- [21] S. Kneip *et al.*, Bright spatially coherent synchrotron x-rays from a table-top source, *Nat. Phys.* **6**, 980 (2010).
- [22] K. T. Phuoc, S. Corde, C. Thauray, V. Malka, A. Tafzi, J.-P. Goddet, R. C. Shah, S. Sebban, and A. Rousse, All-optical Compton gamma-ray source, *Nat. Photonics* **6**, 308 (2012).
- [23] N. D. Powers, I. Ghebregziabher, G. Golovin, C. Liu, S. Chen, S. Banerjee, J. Zhang, and D. P. Umstadter, Quasi-monoenergetic and tunable x-rays from a laser-driven Compton light source, *Nat. Publishing Group* **8**, 28 (2013).
- [24] K. Khrennikov, J. Wenz, A. Buck, J. Xu, M. Heigoldt, L. Veisz, and S. Karsch, Tunable all-optical quasimonochromatic thomson x-ray source in the nonlinear regime, *Phys. Rev. Lett.* **114**, 195003 (2015).
- [25] E. Esarey, C. B. Schroeder, and W. P. Leemans, Physics of laser-driven plasma-based electron accelerators, *Rev. Mod. Phys.* **81**, 1229 (2009).
- [26] A. Gonsalves, B. Pollock, and W. Lu, Summary report of working group 1: Laser-plasma wakefield acceleration, *AIP Conf. Proc.* **1812**, 030001 (2017).
- [27] R. Shaloo, Hydrodynamic optical-field-ionized plasma waveguides for laser plasma accelerators, Ph.D. thesis, University of Oxford, 2018.
- [28] R. J. Shaloo, C. Arran, L. Corner, J. Holloway, J. Jonnerby, R. Walczak, H. M. Milchberg, and S. M. Hooker, Hydrodynamic optical-field-ionized plasma channels, *Phys. Rev. E* **97**, 053203 (2018).
- [29] R. J. Shaloo, C. Arran, A. Picksley, A. V. Boetticher, L. Corner, J. Holloway, G. Hine, J. Jonnerby, H. M. Milchberg, C. Thornton, R. Walczak, and S. M. Hooker, Low-density hydrodynamic optical-field-ionized plasma channels generated with an axicon lens, *Phys. Rev. Accel. Beams* **22**, 041302 (2019).
- [30] C. G. Durfee and H. M. Milchberg, Light pipe for high intensity laser pulses, *Phys. Rev. Lett.* **71**, 2409 (1993).
- [31] C. G. Durfee, F. Lynch, and H. M. Milchberg, Mode properties of a plasma waveguide for intense laser pulses: erratum, *Opt. Lett.* **20**, 946 (1995); C. G. Durfee, F. Lynch, and H. M. Milchberg, Mode properties of a plasma waveguide for intense laser pulses, *Opt. Lett.* **19**, 1937(E) (1994).
- [32] T. R. Clark and H. M. Milchberg, Time- and space-resolved density evolution of the plasma waveguide, *Phys. Rev. Lett.* **78**, 2373 (1997).
- [33] V. Kumarappan, K. Y. Kim, and H. M. Milchberg, Guiding of intense laser pulses in plasma waveguides produced from efficient, femtosecond end-pumped heating of clustered gases, *Phys. Rev. Lett.* **94**, 205004 (2005).
- [34] A. Picksley, A. Alejo, R. J. Shaloo, C. Arran, A. von Boetticher, L. Corner, J. A. Holloway, J. Jonnerby, O. Jakobsson, C. Thornton, R. Walczak, and S. M. Hooker, Meter-scale, conditioned hydrodynamic optical-field-ionized plasma channels, *Phys. Rev. E* **102**, 053201 (2020).
- [35] A. Picksley, A. Alejo, J. Cowley, N. Bourgeois, L. Corner, L. Feder, J. Holloway, H. Jones, J. Jonnerby, H. M. Milchberg, L. R. Reid, A. J. Ross, R. Walczak, and S. M. Hooker, Guiding of high-intensity laser pulses in 100 mm-long hydrodynamic optical-field-ionized plasma channels, *Phys. Rev. Accel. Beams* **23**, 081303 (2020).
- [36] B. Miao, L. Feder, J. E. Shrock, A. Goffin, and H. M. Milchberg, Optical guiding in meter-scale plasma waveguides, *Phys. Rev. Lett.* **125**, 074801 (2020).
- [37] L. Feder, B. Miao, J. E. Shrock, A. Goffin, and H. M. Milchberg, Self-waveguiding of relativistic laser pulses in neutral gas channel, *Phys. Rev. Res.* **2**, 043173 (2020).
- [38] A. Alejo, J. Cowley, A. Picksley, R. Walczak, and S. Hooker, Demonstration of kilohertz operation of hydrodynamic optical-field-ionized plasma channels, *Phys. Rev. Accel. Beams* **25**, 011301 (2022).
- [39] R. H. H. Scott, N. Bourgeois, C. Thornton, J. Cowley, W. Rittershofer, T. Klein, J. Osterhoff, D. R. Symes, C. Hooker, and S. M. Hooker, Electron trapping and re-injection in prepulse-shaped gas targets for laser-plasma accelerators, *Phys. Rev. Accel. Beams* **23**, 111301 (2020).
- [40] K. Oubrierie, A. Leblanc, O. Kononenko, R. Lahaye, I. A. Andriyash, J. Gautier, J.-P. Goddet, L. Martelli, A. Tafzi, K. Ta Phuoc *et al.*, Controlled acceleration of GeV electron beams in an all-optical plasma waveguide, *Light* **11**, 1 (2022).
- [41] B. Miao, J. Shrock, L. Feder, R. Hollinger, J. Morrison, R. Nedbailo, A. Picksley, H. Song, S. Wang, J. Rocca *et al.*, Multi-GeV electron bunches from an all-optical laser wakefield accelerator, *Phys. Rev. X* **12**, 031038 (2022).
- [42] F. M. Foerster *et al.*, Stable and high-quality electron beams from staged laser and plasma wakefield accelerators, *Phys. Rev. X* **12**, 041016 (2022).
- [43] K. v. Grafenstein, F. Foerster, F. Haberstroh, D. Campbell, F. Irshad, F. Salgado, G. Schilling, E. Travac, N. Weiße, M. Zepf *et al.*, Laser-accelerated electron beams at 1 GeV using optically induced shock injection, *Sci. Rep.* **13**, 11680 (2023).
- [44] C. Aniculaesei, H. T. Kim, B. J. Yoo, K. H. Oh, and C. H. Nam, Novel gas target for laser wakefield accelerators, *Rev. Sci. Instrum.* **89**, 025110 (2018).
- [45] See Supplemental Material, which includes Refs. [46–55], at <http://link.aps.org/supplemental/10.1103/PhysRevLett.131.245001> for further details of the laser guiding, electron diagnostics, and the numerical simulations.
- [46] Y. Fournier, J. Bonelle, C. Moulinec, Z. Shang, A. Sunderland, and J. Uribe, Optimizing code_saturne computations on petascale systems, *Comput. Fluids* **45**, 103 (2011).
- [47] code_saturne, <https://www.code-saturne.org/cms/web/>, accessed 2023-07-24.
- [48] A. Popp, J. Vieira, J. Osterhoff, Z. Major, R. Hörlein, M. Fuchs, R. Weingartner, T. P. Rowlands-Rees, M. Marti, R. A. Fonseca, S. F. Martins, L. O. Silva, S. M. Hooker, F. Krausz, F. Grüner, and S. Karsch, All-optical steering of laser-wakefield-accelerated electron beams, *Phys. Rev. Lett.* **105**, 215001 (2010).
- [49] T. D. Arber, K. Bennett, C. S. Brady, A. Lawrence-Douglas, M. G. Ramsay, N. J. Sircombe, P. Gillies, R. G. Evans, H. Schmitz, A. R. Bell, and C. P. Ridgers, Contemporary particle-in-cell approach to laser-plasma modelling, *Plasma Phys. Controlled Fusion* **57**, 113001 (2015).
- [50] B. Fryxell, K. Olson, P. Ricker, F. X. Timmes, M. Zingale, D. Q. Lamb, P. MacNeice, R. Rosner, J. W. Truran, and H. Tufo, FLASH: An adaptive mesh hydrodynamics code for

- modeling astrophysical thermonuclear flashes, *Astrophys. J. Suppl. Ser.* **131**, 273 (2000).
- [51] R. Lehe, M. Kirchen, I. A. Andriyash, B. B. Godfrey, and J. L. Vay, A spectral, quasi-cylindrical and dispersion-free particle-in-cell algorithm, *Comput. Phys. Commun.* **203**, 66 (2016).
- [52] S. Jalas, I. Dornmair, R. Lehe, H. Vincenti, J.-L. Vay, M. Kirchen, and A. R. Maier, Accurate modeling of plasma acceleration with arbitrary order pseudo-spectral particle-in-cell methods, *Phys. Plasmas* **24**, 033115 (2017).
- [53] A. Huebl, R. Lehe, J.-L. Vay, D. P. Grote, I. Sbalzarini, S. Kuschel, D. Sagan, F. Pérez, F. Koller, and M. Bussmann, openPMD: A meta data standard for particle and mesh based data, <https://github.com/openPMD> (2015).
- [54] M. Kirchen, R. Lehe, B. B. Godfrey, I. Dornmair, S. Jalas, K. Peters, J.-L. Vay, and A. R. Maier, Stable discrete representation of relativistically drifting plasmas, *Phys. Plasmas* **23**, 100704 (2016).
- [55] M. Kirchen, R. Lehe, S. Jalas, O. Shapoval, J.-L. Vay, and A. R. Maier, Scalable spectral solver in galilean coordinates for eliminating the numerical cherenkov instability in particle-in-cell simulations of streaming plasmas, *Phys. Rev. E* **102**, 013202 (2020).
- [56] G. J. Hutchens, Approximate near-field blast theory: A generalized approach, *J. Appl. Phys.* **88**, 3654 (2000).
- [57] H. Suk, N. Barov, J. B. Rosenzweig, and E. Esarey, Plasma electron trapping and acceleration in a plasma wake field using a density transition, *Phys. Rev. Lett.* **86**, 1011 (2001).
- [58] K. Schmid, A. Buck, C. M. S. Sears, J. M. Mikhailova, R. Tautz, D. Herrmann, M. Geissler, F. Krausz, and L. Veisz, Density-transition based electron injector for laser driven wakefield accelerators, *Phys. Rev. Accel. Beams* **13**, 091301 (2010).
- [59] A. Buck, J. Wenz, J. Xu, K. Khrennikov, K. Schmid, M. Heigoldt, J. M. Mikhailova, M. Geissler, B. Shen, F. Krausz, S. Karsch, and L. Veisz, Shock-front injector for high-quality laser-plasma acceleration, *Phys. Rev. Lett.* **110**, 185006 (2013).
- [60] R. D’Arcy, S. Wesch, A. Aschikhin, S. Bohlen, C. Behrens, M. J. Garland, L. Goldberg, P. Gonzalez, A. Knetsch, V. Libov *et al.*, Tunable plasma-based energy dechirper, *Phys. Rev. Lett.* **122**, 034801 (2019).
- [61] Z. Huang and K.-J. Kim, Review of x-ray free-electron laser theory, *Phys. Rev. Accel. Beams* **10**, 034801 (2007).
- [62] C. Emma, X. Xu, A. Fisher, R. Robles, J. MacArthur, J. Cryan, M. Hogan, P. Musumeci, G. White, and A. Marinelli, Terawatt attosecond x-ray source driven by a plasma accelerator, *APL Photonics* **6** (2021).
- [63] H.-E. Tsai, K. K. Swanson, S. K. Barber, R. Lehe, H.-S. Mao, D. E. Mittelberger, S. Steinke, K. Nakamura, J. van Tilborg, C. Schroeder *et al.*, Control of quasi-monoenergetic electron beams from laser-plasma accelerators with adjustable shock density profile, *Phys. Plasmas* **25** (2018).
- [64] K. Swanson, H.-E. Tsai, S. Barber, R. Lehe, H.-S. Mao, S. Steinke, J. Van Tilborg, K. Nakamura, C. Geddes, C. Schroeder *et al.*, Control of tunable, monoenergetic laser-plasma-accelerated electron beams using a shock-induced density downramp injector, *Phys. Rev. Accel. Beams* **20**, 051301 (2017).
- [65] L. Fan-Chiang, H.-S. Mao, H.-E. Tsai, T. Ostermayr, K. Swanson, S. Barber, S. Steinke, J. Van Tilborg, C. Geddes, and W. Leemans, Gas density structure of supersonic flows impinged on by thin blades for laser-plasma accelerator targets, *Phys. Fluids* **32** (2020).